Published in final edited form as:
Mol Cell. 2010 August 13; 39(3): 421–432. doi:10.1016/j.molcel.2010.07.022.

Phospholipase D2-dependent Inhibition of the Nuclear Hormone Receptor PPARγ by Cyclic Phosphatidic Acid

Tamotsu Tsukahara[1,*,#], **Ryoko Tsukahara**[1,#], **Yuko Fujiwara**[1], **Junming Yue**[1], **Yunhui Cheng**[1,**], **Huazhang Guo**[1], **Alyssa Bolen**[1], **Chunxiang Zhang**[2,**], **Louisa Balazs**[3], **Fabio Re**[4], **Guangwei Du**[5,***], **Michael A. Frohman**[5], **Daniel L. Baker**[6], **Abby L. Parrill**[6,7], **Ayako Uchiyama**[8], **Tetsuyuki Kobayashi**[8], **Kimiko Murakami-Murofushi**[8], and **Gabor Tigyi**[1]

[1] Department of Physiology, University of Tennessee Health Science Center Memphis, Memphis, TN, 38163, USA

[2] Department of Medicine, University of Tennessee Health Science Center Memphis, Memphis, TN, 38163, USA

[3] Department of Pathology, University of Tennessee Health Science Center Memphis, Memphis, TN, 38163, USA

[4] Department of Molecular Sciences, University of Tennessee Health Science Center Memphis, Memphis, TN, 38163, USA

[5] Center for Developmental Genetics and Department of Pharmacology, Stony Brook University, Stony Brook, NY 11794, USA

[6] Department of Chemistry, University of Memphis, TN 38152, USA

[7] Computational Research on Materials Institute, University of Memphis, TN 38152, USA

[8] Department of Biology, Ochanomizu University, Tokyo 112-8610, Japan

Summary

Cyclic phosphatidic acid (1-acyl-2,3-cyclic-glycerophosphate, CPA), one of nature's simplest phospholipids, is found in cells from slime mold to humans and has largely unknown function. We find here that CPA is generated in mammalian cells in a stimulus coupled-manner by Phospholipase D2 (PLD2), and binds to and inhibits the nuclear hormone receptor PPARγ with nanomolar affinity and high specificity through stabilizing its interaction with the corepressor SMRT. CPA production inhibits the PPARγ target-gene transcription that normally drives adipocytic differentiation of 3T3-L1 cells, lipid accumulation in RAW264.7 cells and primary mouse macrophages, and arterial wall remodeling in a rat model *in vivo*. Inhibition of PLD2 by shRNA, a dominant negative mutant, or a small molecule inhibitor blocks CPA production and

Contact: Gabor Tigyi, M.D., Ph.D., Dept. of Physiology, UTHSC, 894 Union Avenue, Memphis, TN 38163, Tel.: 901-448-4793, Fax: 901-448-7126, gtigyi@physio1.uthsc.edu.
[#]Contributed equally.
[*]Present address: Department of Integrative Physiology & Bio-System Control, Shinshu University School of Medicine, 3-1-1 Asahi, Matsumoto 390-8621, Japan
[**]Present address: Department of Anesthesiology, University of Medicine & Dentistry of New Jersey, Newark, NJ 07101-1709
[***]Present address: Department of Integrative Biology and Pharmacology University of Texas Health Science Center at Houston, Houston, TX 77030

Conflict of interest statement: GT is a founder of RxBio Inc.

relieves PPARγ inhibition. We conclude that CPA is a second messenger and a physiological inhibitor of PPARγ, revealing that PPARγ is regulated by endogenous agonists as well as by antagonists.

INTRODUCTION

PPARγ plays an essential role in regulating lipid and glucose homeostasis, cell proliferation, apoptosis, and inflammation (Ricote and Glass, 2007; Tontonoz and Spiegelman, 2008). These pathways have a direct impact on human diseases, in particular in diabetes (Lehmann et al., 1995), atherosclerosis (Li et al., 2000), and cancer (Sarraf et al., 1998). Synthetic agonists of PPARγ include the thiazolidinedione (TZD) class of drugs, which are widely used to improve insulin sensitivity in type 2 diabetes. Physiological agonists of PPARγ include 15d-PGJ_2 (Forman et al., 1995), modified fatty acids (Li et al., 2008; Nagy et al., 1998), select species of lysophosphatidic acid (1-acyl-2-hydroxy-*sn*-glycero-3-phosphate, LPA; Fig. 1a) (McIntyre et al., 2003), and oxidized phospholipids (Tontonoz et al., 1998). Another phospholipid, 1-palmitoyl-2-oleoyl-sn-glycerol-3-phosphocholine has recently been recognized as a physiologically relevant agonist of PPARα (Chakravarthy et al., 2009). Despite the beneficial effects of PPARγ on glucose and lipid homeostasis, excess PPARγ activity can be deleterious. PPARγ agonists promote adipocytic differentiation of 3T3-L1 cells and also stimulate the uptake of low-density lipoprotein (LDL) by macrophages, leading to foam cell formation in the arterial wall (Moore et al., 2001; Tontonoz et al., 1998). When applied topically to the carotid arterial wall in rodents, select molecular species of LPA and the TZD drug rosiglitazone (ROSI) induce PPARγ-mediated intimal thickening (Cheng et al., 2009; Zhang et al., 2004). Alkyl-ether analogs of LPA accumulate in the atherogenic oxidized-LDL (Zhang et al., 2004) and human atherosclerotic plaques (Rother et al., 2003), and are potent agonists of PPARγ (Tsukahara et al., 2006). This led us to hypothesize that select LPA analogs could be endogenous regulators of PPARγ; hence, we investigated the structure-activity relationship of activation by naturally occurring lysophospholipids (Fig. 1a).

RESULTS

CPA is a specific and a high-affinity antagonist of PPARγ

When testing lysophospholipids using a PPARγ reporter gene assay, we observed that CPA at concentrations as high as 5 μM failed to activate transcription (Fig. 1b). In contrast, LPA 18:1 and its ether analog alkyl glycerol phosphate (AGP 18:1) strongly activated PPARγ. Smaller chemical components of CPA, namely oleoyl glycerol (OG), octadecyl glycerol (AG), and oleic acid (OA) showed weak activation. Exogenously applied CPA species inhibited PPARγ-dependent gene expression elicited by TZDs ROSI (Fig. 1c), pioglitazone and troglitazone (Fig. S1a–b) in a cell-based PPARγ reporter gene assay. The highly homologous PPARα and PPARβ/δ receptors were neither inhibited nor activated by CPA (Fig. S1c–f). To establish a direct interaction between CPA and the PPARγ ligand-binding domain (LBD), recombinant LBD was purified to examine the displacement of agonists [^{3}H]-ROSI (Fig. 1d) and [^{32}P]-AGP (Fig. 1e) by CPA. CPA and its ether analog 1-O-octadecyl-2,3-cyclic-glycerophosphate (CGP 18:1, Fig. 1a) displaced both labeled agonists, and Scatchard analysis revealed single high-affinity binding constants at 124 ± 19 nM and 172 ± 27 nM, respectively (Fig. 1f), which was comparable to that of ROSI (84 ± 6 nM). To monitor the metabolic fate and distribution of exogenously applied CPA, we synthesized a fluorescent analog BODIPY-CPA (Fig. 1a), which also displaced [^{3}H]-ROSI from the PPARγ-LBD (Fig 1g). BODIPY-CPA was applied to RAW267.4 macrophages and uptake of the fluorescent lipid was determined as a function of time. BODIPY-CPA uptake peaked at 15 min before beginning to undergo metabolism by deacylation into BODIPY-fatty acid

(Fig. 1h), whereas no BODIPY-LPA or any other metabolic product was detectable, indicating the stability of the cyclic-phosphate ring. The cellular half-life of BODIPY-CPA in this experiment was approximately 60 min (Fig. 1i) and the label was present in both the cytoplasm and nuclei of the cells after 30 min (Fig. 1j).

Differential interactions between agonists and the antagonist CPA with the PPARγ-LBD

The crystal structures of the PPARγ-LBD and the ROSI-bound complex have previously been solved (Nolte et al., 1998). Currently no reported studies on antagonist-bound structures of the PPARγ-LBD are available in the public domain. Using a crystal structure of the highly homologous PPARα bound to antagonist GW6471, we generated a homology model of the inactive PPARγ-LBD complex. The active-LBD and inactive-LBD served as targets in computational docking studies with ROSI, AGP 18:1, and CPA 18:1 (Fig. 2a–b). CPA 18:1 forms ion-pairing interactions with residue R288 that was previously shown to interact with AGP 18:1 in the PPARγ-LBD (Tsukahara et al., 2006). This interaction is required for binding of the phosphate-containing agonists. However, only the alkyl chain of AGP 18:1 showed favorable interactions with a hydrophobic residue of the AF-12 helix, L469, in the active-LBD (Fig 2b). In contrast, CPA 18:1 bound with higher affinity to the inactive-LBD, failing to stabilize the active conformation of the AF-12 helix (Fig. 2a). The docked positions of ROSI and AGP overlap and differ from the docked position of CPA. This is consistent with the agonist activity of ROSI and AGP, and corresponding lack of such activity for CPA. Although CPA does not overlap with the docked position of AGP and ROSI, interactions with common residues occur from a different pocket. These common interactions preclude binding of CPA at the same time as either ROSI or AGP, which explains the competitive antagonistic effect of CPA.

The phosphate group common to LPA and AGP has been previously validated to form a salt bridge with R288 in the LBD (Tsukahara et al., 2006). The R288A mutant loses AGP binding and activation; nevertheless, binding to and activation by ROSI remains unchanged (Tsukahara et al., 2006). To evaluate the computationally predicted role of R288 in CPA binding, we expressed its alanine mutant LBD recombinant protein, and examined it for binding to [^{3}H]-ROSI and to [^{32}P]-AGP 18:1 (Fig. 2c–d). The R288A mutant bound [^{3}H]-ROSI but did not bind [^{32}P]-AGP 18:1. Although an excess of unlabeled ROSI, AGP 18:1, or CPA 18:1 competed with [^{3}H]-ROSI binding at the WT PPARγ LBD, only ROSI displaced the labeled ligand in the R288A mutant. These results confirm the critical role of the predicted salt bridge between residue R288 and CPA 18:1 and support the hypothesis that CPA functions as a high-affinity antagonist of PPARγ.

The inactive conformation of PPARγ promotes binding of corepressor proteins. Antagonists should prevent the agonist-induced dissociation of this complex. Using a two-hybrid assay (Yu et al., 2005) in CV-1 cells that allows detection of the complex formed between PPARγ and its corepressor SMRT, we tested the effect of CPA on ROSI-induced dissociation of this molecular complex. CPA and CGP dose-dependently stabilized the SMRT-PPARγ and antagonized ROSI-induced dissociation of the complex (Fig. 2e).

Activation of PLD2 generates CPA

CPA has been detected in mammalian tissues (Murakami-Murofushi et al., 2000). To establish a physiological role for CPA in the regulation of PPARγ, we determined whether cellular activation of phospholipase D (PLD) can generate it because prior work showed that the catalytic mechanism of PLD from *Streptomyces chromofuscus* includes CPA as a reaction intermediate (Friedman et al., 1996). MDA-MB-231 breast cancer cells, which express both the PLD1 and PLD2 isoenzymes (Eisen and Brown, 2002), were biosynthetically labeled with [^{32}P]-orthophosphate and stimulated with 100 nM phorbol

myristate acetate (PMA), a strong nonselective activator of both PLD isoforms (Colley et al,. 1997). After 30 min of stimulation, the phospholipids were extracted, separated and compared to phospholipids from vehicle-stimulated cells using two-dimensional thin layer chromatography (2DTLC). No label was detected at the position of an authentic CPA standard spiked into the sample in the vehicle-treated cells (Fig. 2f). In contrast, a spot co-migrating with the CPA standard became detectable in PMA-stimulated cells. The hydrolysis of lysophosphatidyl choline (LPC) by PLD includes a transphosphatidylation step that can be inhibited by the primary alcohol 1-butanol (1-BuOH), but not by secondary alcohol 2-methyl-2-propanol (t-BuOH). When the PMA-stimulated cells were treated with 1-BuOH, the intensity of the [^{32}P]-CPA spot on 2DTLC was significantly reduced, whereas t-BuOH had no effect (Fig. 2f–g).

To determine which of the two PLD isozymes was responsible for CPA production, we used CHO cell lines stably expressing tetracycline-inducible alleles of wild-type (WT) or catalytically-inactive (CI) forms of PLD1 and PLD2 (Du et al., 2004). PMA stimulation of cells with doxycycline (DOX)-induced expression of PLD1 caused a twofold increase in CPA production, which was similar to that observed for WT cells (Fig. 3a). In contrast, DOX-induced PLD2 expression elevated basal levels of CPA and caused a ten-fold increase in PMA-stimulated CPA production relative to non-stimulated WT cells. Expression of the catalytically-inactive PLD2 (CI-PLD2) failed to amplify the PMA-induced CPA production, confirming the requirement for PLD2 activity for the increase in CPA production. In the absence of DOX induction, all four cell lines contained very low amounts of CPA, and PMA stimulation yielded similar increases in CPA (Fig. S2A). These findings suggest that PLD2 activation underlies the stimulus-coupled CPA production.

To obtain direct proof that PLD2 generates CPA, recombinant WT and CI-PLD2 were purified and reacted with [^{14}C]-LPC *in vitro*, and the reaction products separated by TLC (Fig. 3b). WT-PLD2, but not CI-PLD2, generated [^{14}C]-CPA (Vmax = 190 pmol/min/mg; Km = 8 μ M; Fig. S2b). Addition of 1-BuOH to this reaction generated lysophosphatidylbutanol, whereas inclusion of t-BuOH yielded no such product (Fig. 3c–d). These data indicate that mammalian PLD2 is capable of producing CPA from LPC *in vitro* and *in vivo*.

Physiological stimulation of PLD2 generates CPA

CPA levels were then quantified in unstimulated (control) and PMA-stimulated MDA-MB-231 cells by liquid chromatography mass spectrometry (LC-MS). CPA was below the detection limit in control cell extracts (Fig. S2c). Treatment with 100nM PMA for 30 min resulted in the generation of CPA 16:0 and 18:1 (595 ± 1.5 pmol and 293 ± 25.6 pmol/3×10^7 cells, respectively; Fig. S2d). Insulin is a physiological activator of PLD2 (Slaaby et al., 2000). LC-MS quantification of CPA in insulin-stimulated cells showed peak production with 967 ± 111.2 pmol CPA 16:0 and 573 ± 33.5 pmol CPA 18:1 per 3×10^7 cells, respectively (Fig. S2e). Insulin generated higher levels of CPA compared to PMA (Fig. 3e) that peaked at 30 min (Fig. 3f). Insulin stimulation of CV-1 cells did not increase the biosynthetically labeled pool of LPA (Fig. 4a & S3a–c), indicating that the major lysophospholipid product of PLD2 is CPA.

We extended our studies to human peripheral blood mononuclear cells and found that insulin, PMA, lipopolysaccharide (LPS), or H_2O_2 stimulation of PLD2 within 30 minutes caused production of CPA 18:1 and 16:0 (Figs. 4b, S2f–i). In resting monocytes the level of CPA 16:0 and 18:0 was 0.09 and 0.57 pmole/10^7 cells, respectively. After stimulation with 100 nM PMA CPA 16:0 rose ~ 1,400-fold and CPA 18:1 rose ~ 1000-fold (Fig. 4b). Stimulation with 100 nM insulin caused a ~290-fold rise in CPA 18:1. Addition of the PLD2 inhibitor 5-fluoro-2-indolyl des-chlorohalopemide (FIPI 750nM, Su et al., 2009) inhibited

production of both CPA species (Fig. 4b & S2h–i). Thus, physiological stimuli of PLD2 in primary human blood mononuclear cells and also in cultured bone marrow-derived mouse macrophages (data not shown) elicited a rapid and substantial rise of CPA. These results are consistent with the second messenger properties of CPA; very low levels in unstimulated cells, a substantial rise rapidly following PLD2 stimulation, and deacylation-mediated breakdown (Fig. 1i).

Another stimulator of PLD2 is mastoparan. Stimulation of PLD2 with mastoparan or insulin increases CPA production, which in turn should inhibit the transcriptional activity of PPARγ. To test this hypothesis, CV-1 cells were transfected with PPARγ reporter plasmids, and exposed to ROSI with and without stimulation with 20 μM mastoparan or 100 nM insulin (Fig. 4c). Neither PLD-stimulating agent alone caused a significant activation in acetyl CoA-oxidase-luciferase (ACox-luc) reporter gene expression. Rather, mastoparan and insulin both attenuated the ROSI-induced transcriptional activity of PPARγ. When 1-BuOH was added to the cells to quench PLD2-mediated CPA production, the inhibitory effect was attenuated, most strongly for mastoparan (Fig. 4c). Attenuation of ROSI-induced ACox-luc reporter expression positively correlated with the concentration of insulin applied (Fig. 4d).

Insulin stimulates a complex signaling network of which PLD2 activation represents only one component. To obtain evidence that the PLD2 branch of insulin signaling is necessary for CPA production, we treated cells with adenoviral (ad) CI-PLD2, which should abrogate CPA production and the attenuation of PPARγ activation through competing as a dominant-negative isoform with endogenous PLD2. Insulin elicited an increase in the biosynthetically-labeled pool of [^{32}P]-CPA in CV-1 cells, and adCI-PLD2 reduced the insulin-stimulated generation of [^{32}P]-CPA (Fig. 4e). We also probed the requirement of PLD2 for insulin-induced inhibition of PPARγ by using adCI-PLD2 to attenuate CPA production in the reporter gene assay. adCI-PLD2 completely abrogated the inhibitory effect of insulin on PPARγ (Fig. 4f). In addition, we knocked down PLD2 expression using a lentivirally-delivered shRNA against PLD2 in RAW264.7 and NIH3T3-L1 cells (Fig. S3d–f). PLD2 knockdown caused a more than 75% reduction in PMA- and insulin-stimulated CPA 18:1 production in RAW264.7 and 3T3L1 cells (Fig. 5a–b).

CPA and LPA share similar structure. One concern when treating cells with CPA is that CPA may activate LPA GPCR receptors directly before it enters cells. B103 neuroblastoma cells, which express barely detectable levels of PPARγ$_{1\&2}$ (Fig. 5c inset) and also lack the LPA$_{1/2/3}$ GPCR (Tsukahara et al., 2006). Hence, B103 cells represent an ideal cell model for add-back expression of the PPARγ and PPRE-Acox-luc reporter. In wild type B103 cells transfected only with the PPRE-Acox-luc reporter ROSI caused a marginal activation. However, in B103 cells transfected with PPARγ and the reporter, ROSI- or AGP-induced ACox-luc expression that was inhibited by CPA (5 μM) and insulin (1 nM, Fig. 5c). These observations are consistent with the hypothesis that CPA is a physiological product of PLD2 and that PLD2-dependent inhibition of PPARγ activity is mediated by CPA independently of the LPA$_{1/2/3}$ GPCR.

CPA inhibits PPARγ-dependent physiological responses

We also examined the effect of CPA on PPARγ-regulated lipid accumulation in RAW264.7 macrophages after exposure to acetylated low-density lipoprotein (AC-LDL). Uptake of AC-LDL by unstimulated RAW264.7 cells was below the detection limit of the Oil Red O (ORO)-staining (Fig. 5d). When the AC-LDL was co-applied with 5 μM ROSI, many ORO-positive macrophages were visible. CPA (5 μM) addition to ROSI-stimulated macrophages completely abolished ORO-stained cells, supporting the hypothesis that CPA inhibits PPARγ-regulated AC-LDL uptake. The inhibitory effect of CPA on AC-LDL uptake was compared with that of the synthetic PPARγ antagonist GW9662 (Fig. 5e). Both CPA and

GW9662 at 5 μM completely abolished ORO accumulation elicited by either ROSI or AGP in these cells, while causing no change in the expression of PPARγ (Fig. 5e inset). The scavenger receptor CD36, under direct transcriptional regulation of PPARγ, plays an important role in the uptake of oxidized phospholipids into macrophages (Boullier et al., 2000). In CV-1 cells, CPA inhibited ROSI- or AGP-activated *cd36* reporter gene activation only when the reporter construct contained an intact PPARγ response element (PPRE) between nucleotides −273 to −261 in the promoter (Fig. 5f). When the *cd36* promoter was a truncated at position −261, neither ligand showed significant modulation of the expression, which is consistent with the hypothesis that CPA exerts its inhibitory effect on lipid accumulation via the inhibition of PPARγ transcriptional targets. PPARγ is required for adipocytic differentiation of 3T3-L1 cells (Tzameli et al., 2004). In 3T3-L1 cells, 100 nM ROSI treatment elicits the expression of the adipocytic marker FABP4, which is a direct target of PPARγ (Fig. 6a). CPA treatment caused an anti-adipogenic effect evident by the reduced expression of FABP4 mRNA, protein, and by reduced lipid accumulation using ORO staining (Fig. 6b).

Stimulation with low nanomolar insulin leads to PLD2-dependent CPA formation that inhibited PPARγ-dependent reporter gene expression (Fig. 4a–f). To examine the effects of low-dose insulin on adipocytic differentiation, at concentrations similar to that found in plasma under fasting conditions (~ 1 nM), 3T3-L1 cells were induced to differentiate with ROSI for 14 days in the absence or presence of insulin and lipid accumulation quantified using ORO staining (Fig. 6c). Continuous low-dose insulin treatment resulted in the inhibition of adipogenesis as indicated by reduced lipid accumulation, consistent with the dose-response relationship of insulin-induced inhibition of PPARγ-reporter gene activation we found in B103 cells (Fig. 4d). We reasoned that because PLD2 knockdown in 3T3-L1 cells attenuated insulin-activated CPA production (Fig. 5b), it should also reverse the inhibition of PPARγ target genes *fabp4* and *cd36*. PLD2 knockdown reversed insulin or mastoparan inhibition of *fabp4* and *cd36* expression compared to 3T3-L1 cells transduced with scrambled shRNA (Fig. 6d & e).

Stimulation of macrophages with ROSI elicits direct activation of PPARγ-regulated genes (Hodgkinson and Ye, 2003). We selected five PPARγ target genes and monitored their transcriptional regulation in mouse peritoneal macrophages treated with ROSI in combination with CPA or GW9662 for 12h. ROSI stimulation activated the expression of *cd36, cyp27a1, hadh* and *capn3* by 3- to 4-fold, whereas inhibited the expression of *csf1*. CPA as well as GW9662 completely abolished the transcriptional regulation of these genes by ROSI (Fig. 6f).

To examine the regulatory role of CPA on a PPARγ-dependent pathophysiological response we utilized a rodent model of vascular remodeling. ROSI and AGP induce neointima when applied topically within the carotid artery (Zhang et al., 2004). Neointima formation requires PPARγ because it is abolished by the antagonist GW9662 and is absent in mice with conditional knockout of PPARγ targeted to cells of the vessel wall (Cheng et al., 2009). We hypothesized that co-application of CPA with the PPARγ agonists AGP or ROSI should mitigate neointimal thickening. AGP or ROSI with or without CPA was injected lumenally into the common carotid artery of rats, which had been transiently ligated proximally and distally from the carotid glomus. After a 1 h treatment, the cannula was withdrawn and blood flow through the common carotid artery restored. Histological evaluation of the dissected common carotid arteries 3 weeks later revealed multilayered neointimal thickening in the rats treated with 5 μM AGP (Fig. 7a) or ROSI (Fig. S4b) whereas, no neointima was found in the solvent-treated carotids (Fig. S4a). The neointimal thickening was abolished in those animals that received 5 μM CPA in addition to AGP or ROSI (Fig. 7b–c, Fig. S4c–d). Our experiments identified insulin as a physiologically relevant stimulator of CPA

production. Therefore, endogenous production of CPA activated by low concentrations of insulin should prevent neointima formation in this model. To test this possibility, we co-applied 3 nM insulin with 10 μM AGP or ROSI lumenally for 1 h using the same experimental paradigm described for the application of CPA. Examination of the intima-to-media ratio three weeks later showed that low-dose insulin treatment alone induced no vascular remodeling, but insulin co-treatment significantly reduced the neointima formation elicited by AGP or ROSI (Fig. 7d–f, Fig. 4e–g). These results are consistent with the hypothesis that exogenously applied or endogenously generated CPA is effective in negatively modulating PPARγ-dependent vascular wall responses *in vivo*.

DISSCUSSION

The present findings provide evidence that CPA is a *bona fide* second messenger and a negative physiological regulator of PPARγ. CPA is a high-affinity ligand of PPARγ with an apparent Kd in the hundred-nanomolar range, comparable to that of TZDs. CPA binds to a site within the LBD that prevents activation by three different TZD compounds and the endogenous phospholipid agonist AGP, and it stabilizes binding of the co-repressor SMRT. CPA lacks the ability to activate PPARγ due to its cyclic phosphate moiety. In contrast, AGP and LPA both possess a free phosphate and are agonists of PPARγ (Tsukahara et al., 2006). CPA is barely detectable in resting cells but is generated intracellularly in a stimulus-coupled manner by PLD2 and is then degraded by phospholipase(s) or acyltransferase(s) via deacylation. PLD2 is the target and convergence point of several receptor-coupled signal transduction pathways (Huang and Frohman, 2007), suggesting that PPARγ is modulated by stimuli of this enzyme. The present findings establish that PLD2 can produce at least two second messengers, PA from the hydrolysis of phosphatidylcholine and CPA from LPC, depending on substrate availability. The availability of LPC is likely to be regulated by activation of phospholipases A2, which are concomitantly activated by the same stimuli that activate PLD2 (Kim et al., 1999). Physiological stimuli of PLD2 can generate CPA in biologically effective concentrations, as indicated by our findings using the foam-cell formation and adipocyte differentiation models in cultured cell lines and also using primary monocytes/macrophages, and PPARγ-dependent vascular remodeling *in vivo*. In addition, the present data reinforce the long-standing observation that low concentrations of insulin protect against neointimal growth (Breen et al., 2009).

Current paradigms for PPARγ signaling do not take into consideration the possibility of endogenous negative regulators fine-tuning, and under certain conditions even abrogating the cellular responses mediated through this nuclear hormone receptor. Our findings challenge this view by identifying CPA as an endogenous negative regulator of PPARγ. Individual variations in patients in the activation of the PLD2-CPA axis are likely to modulate therapeutic responses to the widely used class of TZD drugs targeting PPARγ. Hence, the present results provide new grounds for rethinking our current concepts governing the regulation of this nuclear hormone receptor and raise the possibility of utilizing this phospholipid scaffold as a lead for the synthesis of new medicines acting on PPARγ.

EXPERIMENTAL PROCEDURES

Cells

All cell lines were from ATCC unless stated otherwise. MDA-MB-231 cells were grown in Leibovitz's L-15 medium (Invitrogen) containing 10% (v/v) FBS, 100 U/ml penicillin, and 10 μg/ml streptomycin. CV-1, B103 (rat neuroblastoma cells, from Dr. Jerold Chun, Scripps Institute, La Jolla, CA), RAW264.7 mouse macrophage cells and 3T3-L1 mouse fibroblast cells were grown in Dulbecco's modified Eagle's medium containing 10% FBS, penicillin,

streptomycin, and 1 mM sodium pyruvate. Tetracycline operator-regulated PLD1 and PLD2 transfected CHO have been characterized elsewhere (Du et al., 2004) and were grown in Ham's F12 medium with 5% FBS. Induction of PLD expression was done by 1.5 μg/ml doxycycline (Sigma) for 24 h. Sf-9 insect cells (Invitrogen) were grown in serum-free medium Sf-900 II (Invitrogen).

Ligand-Binding Assays

Ligand binding assays were preformed as described in detail previously (Tsukahara et al., 2006).

PPAR Reporter Gene Assays

Determination of PPARα, β/δ, and γ activation was done in CV-1 cells (endogenously express $LPA_{1/2/3}$) or B103 cells (lack endogenous $LPA_{1/2/3}$ receptors and PPARγ) transfected with 125 ng of the appropriate reporter gene (pGL3-PPRE–acyl-CoA oxidase luciferase or in some experiments with MH100-PPRE-TK-luciferase) and 62.5 ng of pcDNA3.1-PPARγ or pCMX-PPARγ-Gal4 and 12.5 ng of pSV–β-galactosidase (Promega) construct as previously reported (Tsukahara et al., 2006). To monitor activation of PPARα, 62.5 ng of pG4M-PPARα-ligand binding domain and 12.5 ng of pSV- β-galactosidase or 125 ng of 17 m5 ×-βGLOB-luc plasmids were transfected into B103 cells using Lipofectamine 2000. For PPAR β/δ, we used 62.5 ng of pG4M-PPAR β/δ-LBD plasmid DNA and 12.5 ng of pSV- β -galactosidase or 125 ng of 17 m5×-βGLOB-luc plasmids. Twenty-four hours after transfection, cells were treated with Opti-MEM containing 10 μ M test compound dissolved in DMSO and cultured for an additional 20 h. Luciferase activity was measured with the Steady-Glo Luciferase Assay System (Promega) using a Fusion Alpha plate reader (Perkin-Elmer).

Co-repressor two-hybrid assays

The effect of CPA on SMRT co-repressor binding to PPARγ was done as described by Yu et al. (Yu et al., 2005). Briefly, CV-1 cells were plated onto 96-well plate at the density of 1.0×10^4 cells per well in DMEM containing 10% FBS. The next day, the cells were transiently transfected with 71 ng of UAS-Luc, 14.3 ng of Gal4-SMRT, 14.3 ng of pVP16-PPARγ2, and 10 ng of pSV–βgalactosidase (Promega) using Lipofectamine LTX (Invitrogen). Twenty hours after transfection, the cells were pretreated with various concentrations of CPA or CGP 18:1 in Opti-MEM (Invitrogen) for 30 min, followed by treated with Opti-MEM containing 1nM ROSI for 6 h. Luciferase and β-galactosidase activities were measured as above. Samples were run in quintuples, and the mean ± SEM were calculated. Data are representative of at least three independent transfections. Student's *t* test was used to test for statistical analysis and $P<0.05$ was considered significant.

Biosynthetic Labeling of Cells and Measurement of CPA Synthesis

MDA-MB-231 cells (3.5×10^6) or CV-1 cells (10^6) were serum-starved for 12 h and washed with phosphate-free medium and incubated in balanced salt solution (135 mM NaCl, 4.5 mM KCl, 1.5 mM $CaCl_2$, 0.5 mM $MgCl_2$, 5.6 mM glucose, 10 mM HEPES-NaOH, pH7.2) containing 1 mCi/ml [^{32}P]-orthophosphoric acid. After 3 h, the labeling medium was removed, and the cells were washed 3× with Ca^{2+}/Mg^{2+} free phosphate-buffered saline (PBS) and preincubated at 37°C in serum-free medium for 15 min. After treatment with 100 nM PMA (Fluka) for 30 min, the cells were washed once with ice-cold PBS and collected by centrifugation. The phospholipids were extracted (Bligh and Dyer, 1959), spotted on indicator-free high-performance silica gel TLC plates (Whatman) and separated by two-dimensional TLC using chloroform-methanol-acetic acid-1% sodium disulfite (100:40:12:5) solvent in the first dimension and chloroform-methanol-ammonium hydroxide (3:6:1) in the

second dimension. Unlabeled LPA and CPA standards were mixed into the samples and visualized by 0.01% primulin (Sigma) staining, whereas radioactivity was detected by a Cyclone phosphorimager (Perkin-Elmer).

Statistical methods

Significant differences were based on Student's t-test relative to the appropriate control. Equilibrium binding constants (K_D) were calculated from the binding data using the Kaleida-Graph Software version 4.0 (Synergy Software).

Supplementary Material

Refer to Web version on PubMed Central for supplementary material.

Acknowledgments

This work was supported by USPHS Grants, HL79004 (to G. T.) CA92160 (to G.T.), HL 084007 (AP), GM071475 (GD), the American Heart Association Grants 50006N, 355199B (to A. P.), and 0525489B (to T. T.), and National Science Foundation Grant CHE0353885 (to A. P.) and the Quigley Scholarship (RT).

References

Bligh EG, Dyer WJ. A rapid method of total lipid extraction and purification. Can J Biochem Physiol. 1959; 37:911–917. [PubMed: 13671378]

Boullier A, Gillotte KL, Horkko S, Green SR, Friedman P, Dennis EA, Witztum JL, Steinberg D, Quehenberger O. The binding of oxidized low density lipoprotein to mouse CD36 is mediated in part by oxidized phospholipids that are associated with both the lipid and protein moieties of the lipoprotein. J Biol Chem. 2000; 275:9163–9169. [PubMed: 10734051]

Breen DM, Chan KK, Dhaliwall JK, Ward MR, Al Koudsi N, Lam L, De Souza M, Ghanim H, Dandona P, Stewart DJ, et al. Insulin increases reendothelialization and inhibits cell migration and neointimal growth after arterial injury. Arterioscler Thromb Vasc Biol. 2009; 29:1060–1066. [PubMed: 19359661]

Chakravarthy MV, Lodhi IJ, Yin L, Malapaka RR, Xu HE, Turk J, Semenkovich CF. Identification of a physiologically relevant endogenous ligand for PPARalpha in liver. Cell. 2009; 138:476–488. [PubMed: 19646743]

Cheng Y, Makarova N, Tsukahara R, Guo H, Shuyu E, Farrar P, Balazs L, Zhang C, Tigyi G. Lysophosphatidic acid-induced arterial wall remodeling: Requirement of PPARgamma but not LPA(1) or LPA(2) GPCR. Cell Signal. 2009

Colley WC, Sung TC, Roll R, Jenco J, Hammond SM, Altshuller Y, Bar-Sagi D, Morris AJ, Frohman MA. Phospholipase D2, a distinct phospholipase D isoform with novel regulatory properties that provokes cytoskeletal reorganization. Curr Biol. 1997; 7:191–201. [PubMed: 9395408]

Du G, Huang P, Liang BT, Frohman MA. Phospholipase D2 localizes to the plasma membrane and regulates angiotensin II receptor endocytosis. Mol Biol Cell. 2004; 15:1024–1030. [PubMed: 14718562]

Eisen SF, Brown HA. Selective estrogen receptor (ER) modulators differentially regulate phospholipase D catalytic activity in ER-negative breast cancer cells. Mol Pharmacol. 2002; 62:911–920. [PubMed: 12237338]

Forman BM, Tontonoz P, Chen J, Brun RP, Spiegelman BM, Evans RM. 15-Deoxy-delta 12, 14-prostaglandin J2 is a ligand for the adipocyte determination factor PPAR gamma. Cell. 1995; 83:803–812. [PubMed: 8521497]

Friedman P, Haimovitz R, Markman O, Roberts MF, Shinitzky M. Conversion of lysophospholipids to cyclic lysophosphatidic acid by phospholipase D. J Biol Chem. 1996; 271:953–957. [PubMed: 8557710]

Gampe RT Jr, Montana VG, Lambert MH, Miller AB, Bledsoe RK, Milburn MV, Kliewer SA, Willson TM, Xu HE. Asymmetry in the PPARgamma/RXRalpha crystal structure reveals the

molecular basis of heterodimerization among nuclear receptors. Mol Cell. 2000; 5:545–555. [PubMed: 10882139]

Goodsell DS, Olson AJ. Automated docking of substrates to proteins by simulated annealing. Proteins. 1990; 8:195–202. [PubMed: 2281083]

Hodgkinson CP, Ye S. Microarray analysis of peroxisome proliferator-activated receptor-gamma induced changes in gene expression in macrophages. Biochem Biophys Res Commun. 2003; 308:505–510. [PubMed: 12914779]

Huang P, Frohman MA. The potential for phospholipase D as a new therapeutic target. Expert Opin Ther Targets. 2007; 11:707–716. [PubMed: 17465727]

Kim JH, Lee BD, Kim Y, Lee SD, Suh PG, Ryu SH. Cytosolic phospholipase A2-mediated regulation of phospholipase D2 in leukocyte cell lines. J Immunol. 1999; 163:5462–5470. [PubMed: 10553072]

Lehmann JM, Moore LB, Smith-Oliver TA, Wilkison WO, Willson TM, Kliewer SA. An antidiabetic thiazolidinedione is a high affinity ligand for peroxisome proliferator-activated receptor gamma (PPAR gamma). J Biol Chem. 1995; 270:12953–12956. [PubMed: 7768881]

Li AC, Brown KK, Silvestre MJ, Willson TM, Palinski W, Glass CK. Peroxisome proliferator-activated receptor gamma ligands inhibit development of atherosclerosis in LDL receptor-deficient mice. J Clin Invest. 2000; 106:523–531. [PubMed: 10953027]

Li Y, Zhang J, Schopfer FJ, Martynowski D, Garcia-Barrio MT, Kovach A, Suino-Powell K, Baker PR, Freeman BA, Chen YE, Xu HE. Molecular recognition of nitrated fatty acids by PPAR gamma. Nat Struct Mol Biol. 2008; 15:865–867. [PubMed: 18604218]

McIntyre TM, Pontsler AV, Silva AR, St Hilaire A, Xu Y, Hinshaw JC, Zimmerman GA, Hama K, Aoki J, Arai H, Prestwich GD. Identification of an intracellular receptor for lysophosphatidic acid (LPA): LPA is a transcellular PPARgamma agonist. Proc Natl Acad Sci U S A. 2003; 100:131–136. [PubMed: 12502787]

Moore KJ, Rosen ED, Fitzgerald ML, Randow F, Andersson LP, Altshuler D, Milstone DS, Mortensen RM, Spiegelman BM, Freeman MW. The role of PPAR-gamma in macrophage differentiation and cholesterol uptake. Nat Med. 2001; 7:41–47. [PubMed: 11135614]

Murakami-Murofushi K, Mukai M, Kobayashi S, Kobayashi T, Tigyi G, Murofushi H. A novel lipid mediator, cyclic phosphatidic acid (cPA), and its biological functions. Ann N Y Acad Sci. 2000; 905:319–321. [PubMed: 10818474]

Nagy L, Tontonoz P, Alvarez JG, Chen H, Evans RM. Oxidized LDL regulates macrophage gene expression through ligand activation of PPARgamma. Cell. 1998; 93:229–240. [PubMed: 9568715]

Nolte RT, Wisely GB, Westin S, Cobb JE, Lambert MH, Kurokawa R, Rosenfeld MG, Willson TM, Glass CK, Milburn MV. Ligand binding and co-activator assembly of the peroxisome proliferator-activated receptor-gamma. Nature. 1998; 395:137–143. [PubMed: 9744270]

Ricote M, Glass CK. PPARs and molecular mechanisms of transrepression. Biochim Biophys Acta. 2007; 1771:926–935. [PubMed: 17433773]

Rother E, Brandl R, Baker DL, Goyal P, Gebhard H, Tigyi G, Siess W. Subtype-selective antagonists of lysophosphatidic Acid receptors inhibit platelet activation triggered by the lipid core of atherosclerotic plaques. Circulation. 2003; 108:741–747. [PubMed: 12885756]

Sarraf P, Mueller E, Jones D, King FJ, DeAngelo DJ, Partridge JB, Holden SA, Chen LB, Singer S, Fletcher C, Spiegelman BM. Differentiation and reversal of malignant changes in colon cancer through PPARgamma. Nat Med. 1998; 4:1046–1052. [PubMed: 9734398]

Slaaby R, Du G, Altshuller YM, Frohman MA, Seedorf K. Insulin-induced phospholipase D1 and phospholipase D2 activity in human embryonic kidney-293 cells mediated by the phospholipase C gamma and protein kinase C alpha signalling cascade. Biochem J. 2000; 351(Pt 3):613–619. [PubMed: 11042115]

Su W, Yeku O, Olepu S, Genna A, Park JS, Ren H, Du G, Gelb M, Morris A, Frohman MA. FIPI, a Phospholipase D pharmacological inhibitor that alters cell spreading and inhibits chemotaxis. Mol Pharmacol. 2009; 75:437–446. [PubMed: 19064628]

Tontonoz P, Nagy L, Alvarez JG, Thomazy VA, Evans RM. PPARgamma promotes monocyte/macrophage differentiation and uptake of oxidized LDL. Cell. 1998; 93:241–252. [PubMed: 9568716]

Tontonoz P, Spiegelman BM. Fat and beyond: the diverse biology of PPARgamma. Annu Rev Biochem. 2008; 77:289–312. [PubMed: 18518822]

Tsukahara T, Tsukahara R, Yasuda S, Makarova N, Valentine WJ, Allison P, Yuan H, Baker DL, Li Z, Bittman R, et al. Different residues mediate recognition of 1-O-oleyllysophosphatidic acid and rosiglitazone in the ligand binding domain of peroxisome proliferator-activated receptor gamma. J Biol Chem. 2006; 281:3398–3407. [PubMed: 16321982]

Tzameli I, Fang H, Ollero M, Shi H, Hamm JK, Kievit P, Hollenberg AN, Flier JS. Regulated production of a peroxisome proliferator-activated receptor-gamma ligand during an early phase of adipocyte differentiation in 3T3-L1 adipocytes. J Biol Chem. 2004; 279:36093–36102. [PubMed: 15190061]

Xu HE, Stanley TB, Montana VG, Lambert MH, Shearer BG, Cobb JE, McKee DD, Galardi CM, Plunket KD, Nolte RT, et al. Structural basis for antagonist-mediated recruitment of nuclear co-repressors by PPARalpha. Nature. 2002; 415:813–817. [PubMed: 11845213]

Yu C, Markan K, Temple KA, Deplewski D, Brady MJ, Cohen RN. The nuclear receptor corepressors NCoR and SMRT decrease peroxisome proliferator-activated receptor gamma transcriptional activity and repress 3T3-L1 adipogenesis. J Biol Chem. 2005; 280:13600–13605. [PubMed: 15691842]

Zhang C, Baker DL, Yasuda S, Makarova N, Balazs L, Johnson LR, Marathe GK, McIntyre TM, Xu Y, Prestwich GD, et al. Lysophosphatidic acid induces neointima formation through PPARgamma activation. J Exp Med. 2004; 199:763–774. [PubMed: 15007093]

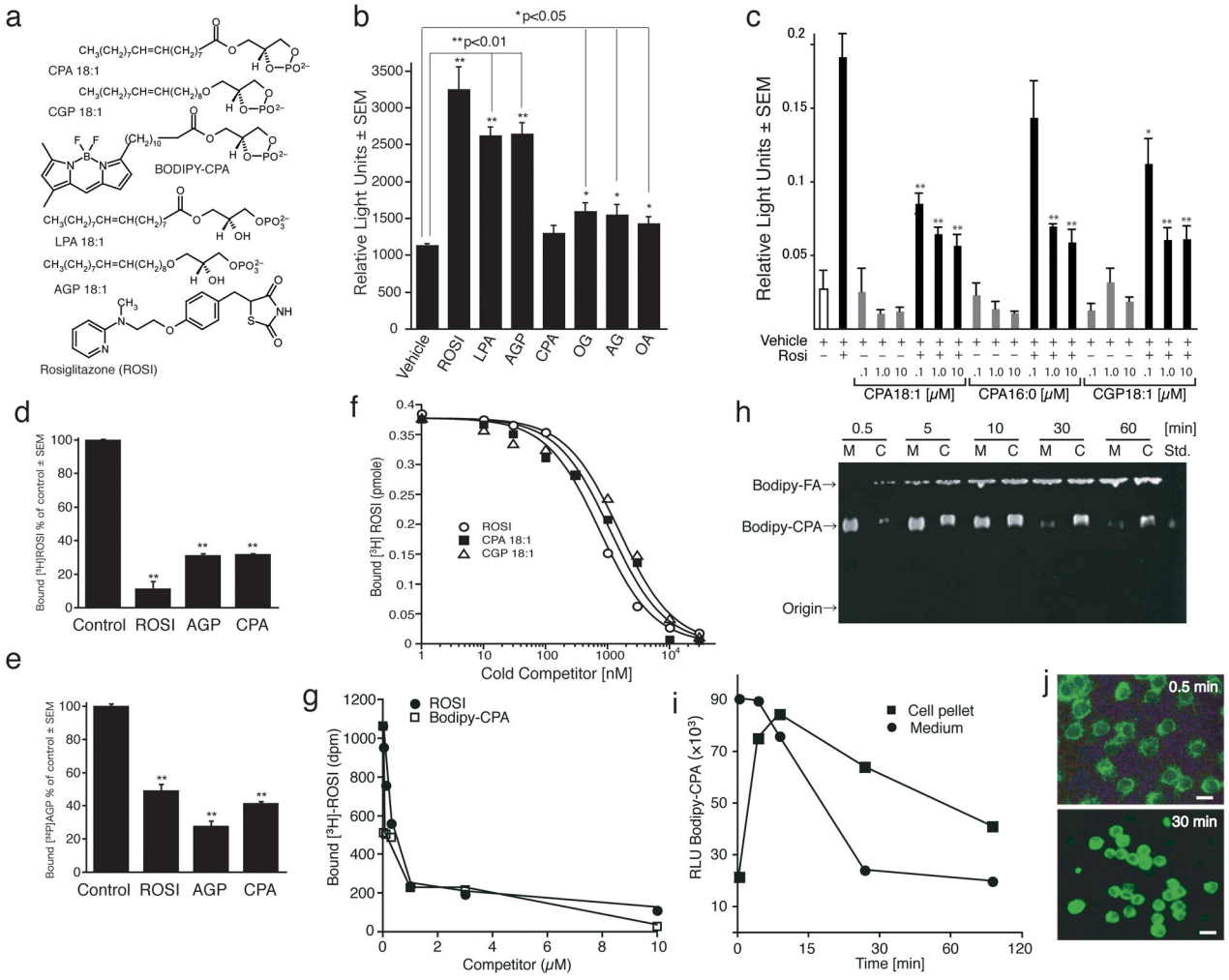

Figure 1. CPA is an antagonist of PPARγ

(a) Structures of the lysophospholipids and ROSI.

(b) CPA does not activate PPARγ-dependent PPRE-ACox-Luc expression. CV-1 cells were transfected with ACox-luc plus pcDNA3.1-PPARγ and treated for 20 h with 5 μM each of ROSI, LPA 18:1, AGP 18:1, CPA 18:1, MG, AG, or OA. Luciferase activities are presented as relative light units (RLU, mean ± SEM, n = 4, *p < 0.05, **p < 0.01).

(c) Different molecular species of CPA and CGP dose-dependently suppress ROSI-induced PPARγ-dependent PPRE-TK-Luc reporter gene activation in B103 cells. B103 cells (3.0×10^4) were transfected with pMH100-PPRE-TK-Luc, pCMX-PPARγ-Gal4, and pSV-β-gal. After transfection, the cells were exposed to CPA or CGP (0.1, 1 and 10 μM) with or without ROSI (10 μM) for 20h, and reporter gene expression measured (mean ± SEM, n=4).

(**d & e**) Competitive displacement of 5 nM [^{3}H]-ROSI or [^{32}P]-AGP from PPARγ-LBD was determined using 2.5 μM cold ROSI, AGP, or CPA.

(f) CPA 18:1 and CGP 18:1 displace [^{3}H]-ROSI from purified LBD of PPARγ. Competition binding was performed using 5 nM [^{3}H]-ROSI and increasing concentrations of CPA or CGP.

(g) BODIPY-CPA competitively displaces [^{3}H]-ROSI from PPARγ LBD. Competition biding assay was performed using purified 3 μg PPARγ-LBD with 5 nM [^{3}H]-ROSI and increasing concentrations of either ROSI or BODIPY-CPA competitor.

(h, i) Uptake of BODIPY-CPA (3 nmoles) into RAW264.7 macrophages. The rate of accumulation and the metabolic fate of labeled CPA was monitored in the medium (M or circles) and macrophages (C or squares) using TLC. The major fluorescent metabolite observed co-migrated with a standard for BODIPY-FA (fatty acid), indicating phospholipase/acyl transferase action. BODIPY-LPA was not detected.
(j) BODIPY-CPA rapidly accumulated in the cell-associated pool and was present in the cytoplasm. Representative fluorescent microscopy image of 3 nmole BODIPY-CPA-treated RAW264.7 macrophages after 0.5 min and 30 min exposure (bar, 50 μm).

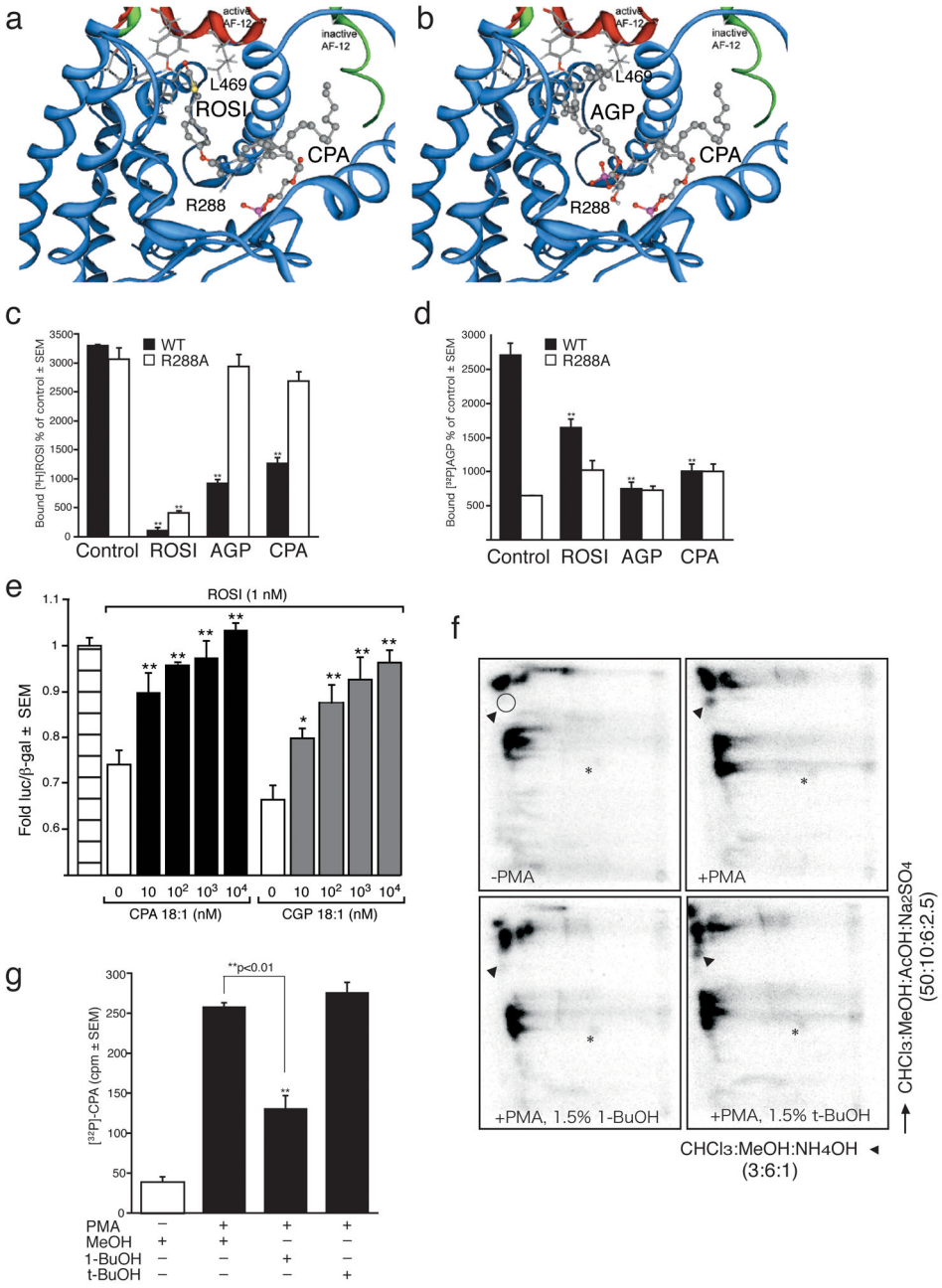

Figure 2. CPA inhibits PPARγ activation and is generated by PLD

(a) Comparison of ROSI crystallized in PPARγ (1FM6) and CPA 18:1 docked into the inactive homology model of PPARγ. Blue ribbons show the backbone structure of the inactive PPARγ homology model. The inactive homology model differs from the active crystallographic structures only in the position of the AF-12 segment, which is shown as a green and a red ribbon in the inactive homology model and the crystallographic structure, respectively. Ligands are shown as ball and stick models.

(b) Comparison of AGP 18:1 docked into the activated crystallographic structure of PPARγ (1FM9) and overlay of CPA 18:1 docked into the inactive homology model of PPARγ. Note that agonists ROSI and AGP occupy the same location and interact with residue R288, while

CPA prevents the AF-12 domain from acquiring its activated conformation (red) by stabilizing the inactivated conformation (green).

(c, d) Arginine 288 is required for inhibition of PPARγ by CPA. Purified WT and R288A mutant PPARγ (1 μg) were incubated with 5 nM [^{3}H]-ROSI or [^{32}P]-AGP 18:1 under equilibrium binding conditions with 2.5 μM cold ROSI, AGP, and CPA, and the bound ligand quantified using a filtration assay (mean ± SEM, n = 4).

(e) ROSI-induced SMRT release from PPARγ is dose-dependently inhibited by both CPA 18:1 and CGP 18:1. CV-1 cells were transfected with UAS-Luc, pECE-Gal4-SMRT (containing full length SMRT), pVP16-PPARγ2, and pSV-β-gal. After transfection, the cells were treated with CPA 18:1 or CGP 18:1 for 30 min, followed by 1nM ROSI for 6 h. Luciferase activities are presented as fold increase (mean ± SEM, n=4, representative of 3 transfections).

(f) Stimulation of biosynthetically [^{32}P]-orthophosphate-labeled MDA-MB-231 cells with PMA (100 nM, 30 min) leads to CPA generation. PMA stimulation (100 nM) was also performed in the presence of either 1.5% 1-BuOH or t-BuOH. Phospholipids were separated using 2D-TLC and visualized using phosphorimaging. Arrows point to the position of the authentic CPA standard and asterisks indicate the position of the LPA standard.

(g) CPA production in PMA-stimulated cells is inhibited by 1-BuOH but not by t-BuOH. Phosphorimaging-based quantification of labeled CPA after stimulation of MDA-MB-231 cells by 100 nM PMA in the presence or not of 1.5% v/v 1-BuOH and t-BuOH (mean cpm ± SEM, n = 4).

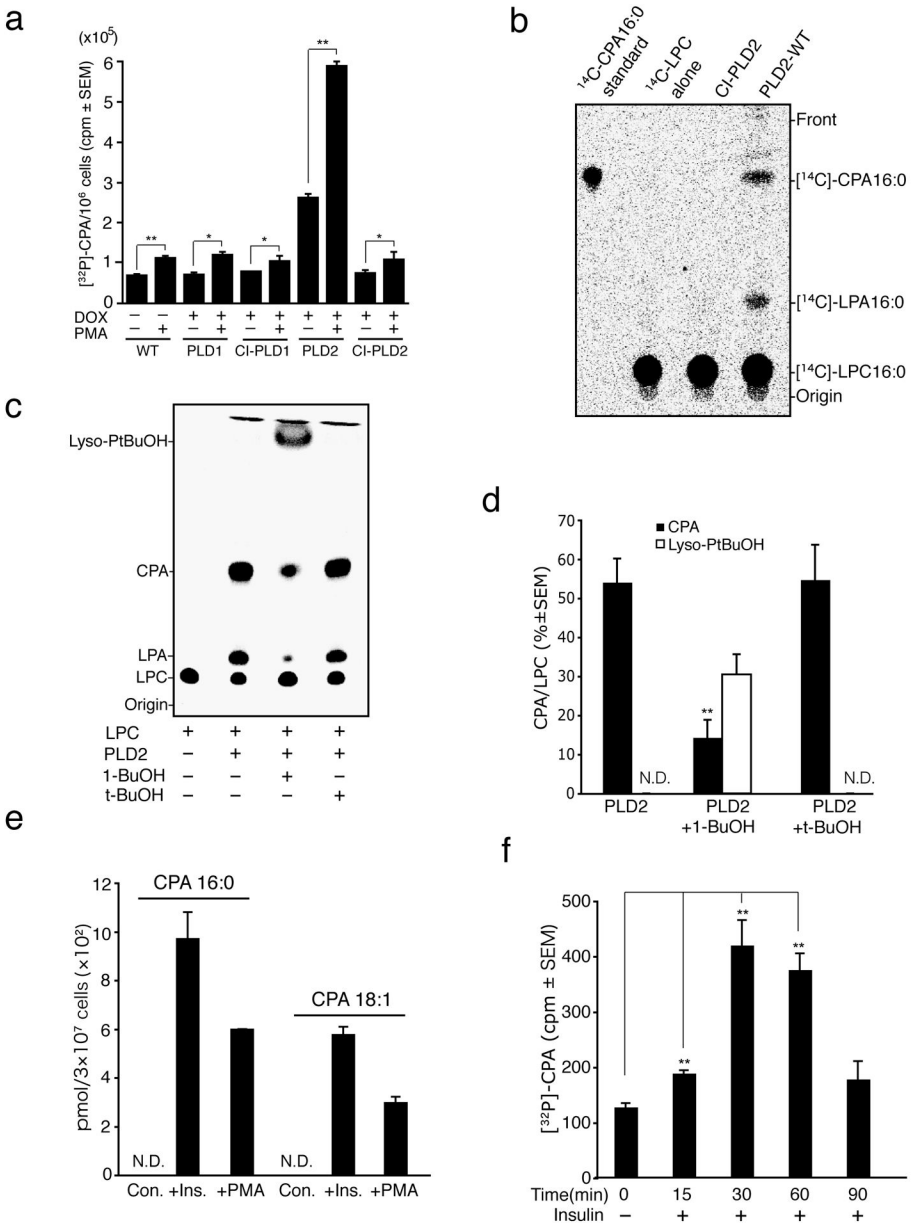

Figure 3. ***In vitro and in vivo*** **generation of CPA by PLD2**

(a) PLD2 is the major source of CPA *in vivo*. CHO cells expressing *tet*-regulated WT or CI-PLD1 or PLD2 constructs were induced by DOX and subsequently stimulated with 100 nM PMA for 30 min. Cellular phospholipids were biosynthetically labeled with 0.1 mCi [^{32}P]-Pi for 12 h, and CPA generation quantified using phosphorimaging after 2D-TLC separation (mean ± SEM, n = 3).

(b) PLD2 generates CPA *in vitro*. Affinity-purified WT or CI-PLD2 (10 μg/reaction) was incubated with [^{14}C]-LPC 16:0 at 40°C for 1 h. The reaction mixtures were spotted on a TLC plate and separated. Authentic cold CPA and LPA standards were used to determine the product Rfs.

(c) 1-BuOH but not t-BuOH diverts recombinant PLD2 formation of CPA to lysophosphatidyl butanol (lyso-PtBuOH). TLC analysis of [^{14}C]-phospholipids generated by purified PLD2 from Sf-9 insect cells after treatment with 0.5% 1-BuOH or t-BuOH.

(d) Quantification of CPA and [^{14}C]-lyso-PtBuOH formation by PLD2 in the presence of 0.5% 1-BuOH and t-BuOH (n = 3). N.D., not detectable.
(e) LC-MS quantification of CPA 16:0 and 18:0 after stimulation of MDA-MB-231 cells by 100 nM insulin or PMA for 30 min (pmol mean ± SEM, n = 3).
(f) Time course of insulin-stimulated CPA production in MDA-MB-231 cells. Cells (3×10^6) biosynthetically labeled with [^{32}P]-orthophosphate were exposed to 100 nM insulin for different times and the CPA purified using 2DTLC and quantified using liquid scintillation counting (n=3).

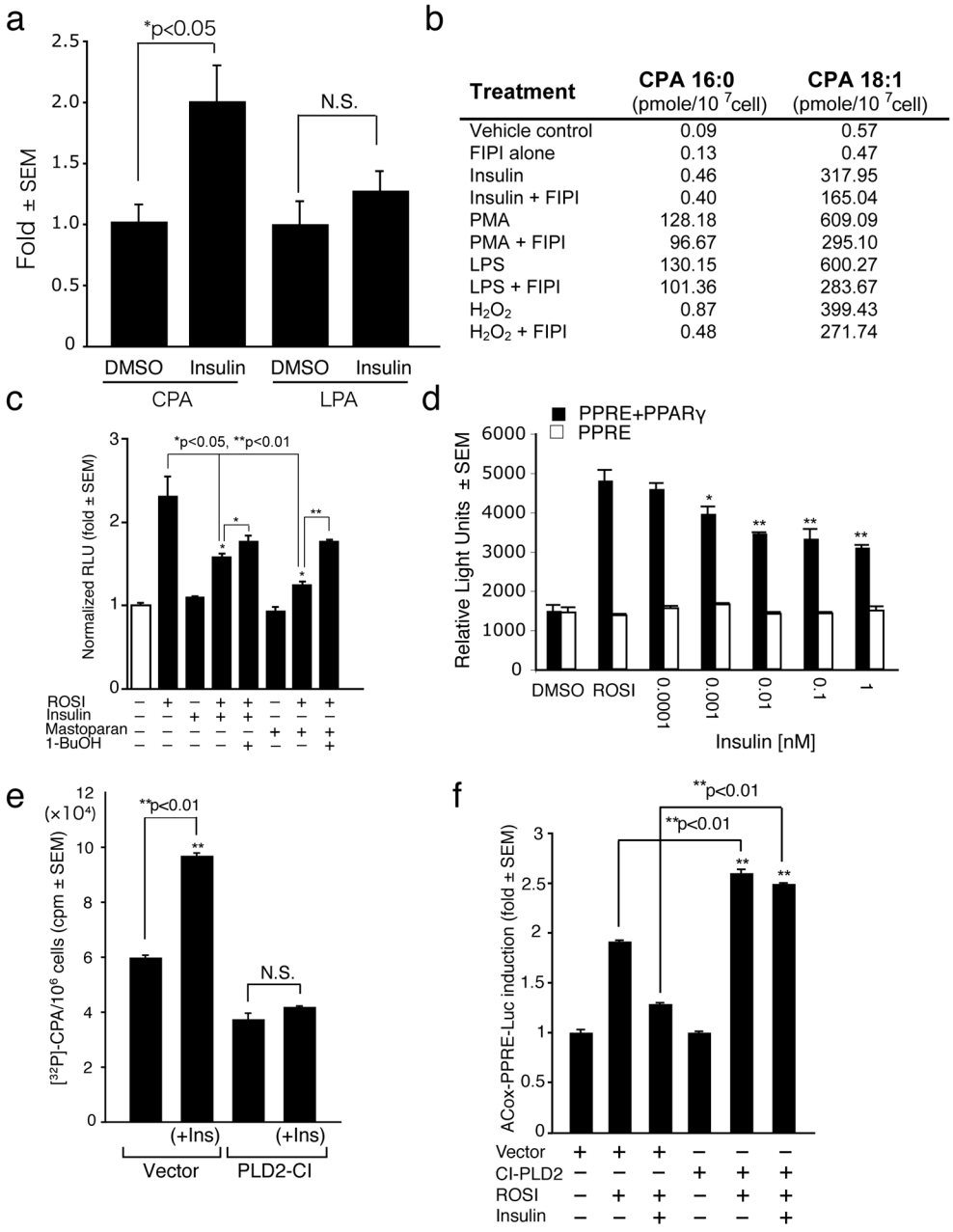

Treatment	CPA 16:0 (pmole/10 ^{7}cell)	CPA 18:1 (pmole/10 ^{7}cell)
Vehicle control	0.09	0.57
FIPI alone	0.13	0.47
Insulin	0.46	317.95
Insulin + FIPI	0.40	165.04
PMA	128.18	609.09
PMA + FIPI	96.67	295.10
LPS	130.15	600.27
LPS + FIPI	101.36	283.67
H_2O_2	0.87	399.43
H_2O_2 + FIPI	0.48	271.74

Figure 4. PLD2 activation inhibits PPARγ

(a) Insulin stimulation elevates CPA but not LPA levels. CV-1 cells (3×10^6) were labeled with [^{32}P]-orthophosphate for 6 h and stimulated with 100 nM insulin or the DMSO solvent for 30 min at 37°C. Lipids were extracted, separated by 2DTLC and quantified by phosphorimaging (n = 3).

(b) CPA is generated in human peripheral blood mononuclear cells in response to PLD2 stimulation. The cells were pretreated with the PLD2 inhibitor FIPI (750 nM) or solvent control for 30 min prior to stimulation by 100 nM insulin, PMA 100 nM, 1 μg/ml LPS, or 1 mM H_2O_2. Data are representative of three other experiments with different donors.

(c) Stimulation of PLD2 with insulin or mastoparan inhibits ROSI-induced PPARγ-reporter gene expression in a PLD-dependent manner. CV-1 cells were transfected with ACox–luc

together with pcDNA3.1-PPARγ plasmid and treated for 20 h with 10 μM ROSI, 100 nM insulin, 20 μM mastoparan, and/or 1.5% 1-BuOH. Luciferase activities are presented as RLU (mean ± SEM, n = 4).

(d) Insulin attenuates PPARγ activation. The ACox-luc reporter alone or in combination with the PPARγ plasmid was transfected into B103 cells and exposed to ROSI (5 μM) alone or with insulin. Reporter gene expression was measured 20h later (n = 5).

(e) CI-PLD2 inhibits insulin-induced CPA production in CV-1 cells. Cells were either transduced with a CI-PLD2 or an empty adenovirus at MOI of 10. Phospholipids were biosynthetically labeled using [^{32}P]-orthophosphate for 24 h post-transduction, and the cells stimulated with 100 nM insulin for 30 min. Phospholipids were separated using 2DTLC and visualized by phosphorimaging. Radioactivity incorporated into the CPA spot was scraped off and quantified by liquid scintillation counting (cpm mean ± SEM, n = 3, **p < 0.01).

(f) CI-PLD2 acts as a dominant negative and abolishes insulin-induced inhibition of ROSI-induced PPARγ activation. CV-1 cells were either transduced with an adCI-PLD2 or an empty adenovirus. Subsequently, the transduced cells were transfected with the ACox-luc reporter gene and PPARγ plasmids for an additional 24 h. Cells were stimulated with 10 μM ROSI with or without 100 nM insulin for 20 h, and luciferase reporter expression determined (mean ± SEM, n=3, **p < 0.01).

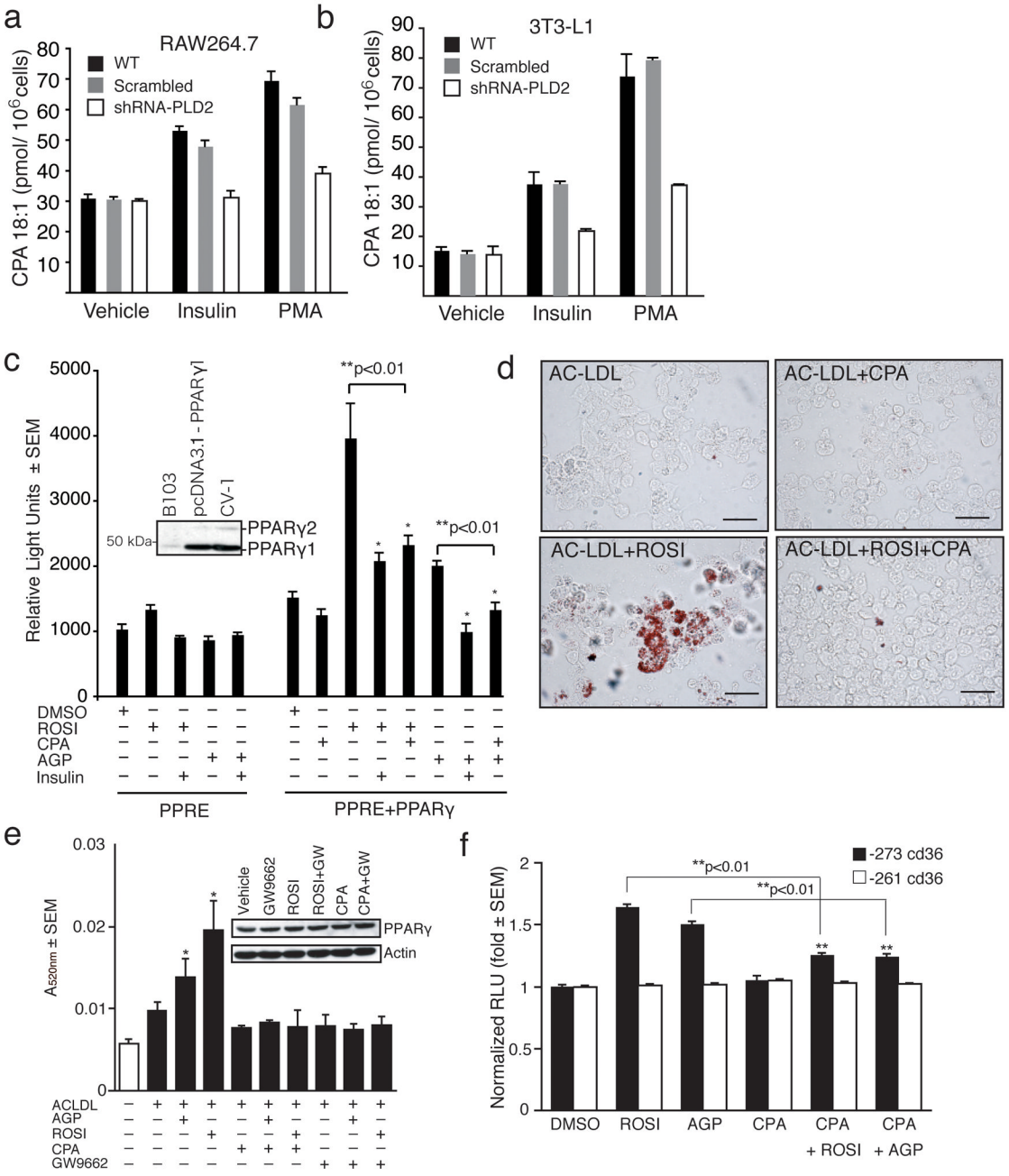

Figure 5. CPA production by PLD2 inhibits PPARγ-mediated cellular responses

(a & b) PLD2 knockdown inhibits insulin- and PMA-induced CPA production in RAW264.7 and 3T3-L1 cells. 3 × 10^6 RAW264.7 or NIH3T3 cells expressing scrambled shRNA or PLD2 shRNA were stimulated with 30 nM insulin or 100 nM PMA for 30 min prior to extraction of phospholipids for MS analysis (n=3).

(c) B103 cells were transfected with the ACox-luc reporter gene alone or together with the PPARγ plasmid and exposed to ROSI (5 μM) with or without CPA (5 μM), AGP (5 μM) and insulin (1 nM) for 20 h, and reporter gene expression measured (mean ± SEM, n = 3). The inset shows PPARγ expression in WT B103 cells or cells transfected with the pcDNA3.1- PPARγ construct as determined by western blotting.

(d) CPA inhibits foam cell formation and AC-LDL accumulation in the RAW264.7 mouse macrophage cell line. Cells were stimulated with combinations of 5 μM CPA and ROSI in the presence of 25 μg/ml AC-LDL for 24 h. Lipid accumulation was determined by ORO staining (bar = 50 μm).
(e) CPA and the PPARγ antagonist GW9662 (5 μM each) inhibited ROSI- and AGP-induced (5 μM each) lipid accumulation in RAW264.7 macrophages. ORO accumulation was quantifed spectrophotometrically (mean ± SEM, n = 3). The inset shows PPARγ expression as assessed by western blotting and the lower panel shows β-actin as a loading control.
(f) CPA inhibition of PPARγ target gene *cd36* activation requires a PPRE element. CV-1 cells were transfected with PPARγ together with a *cd36* reporter gene containing PPRE at position −273 in the promoter, or a truncated version at position −261 lacking the PPRE, and were treated for 20 h with 10 μM ROSI, AGP, or CPA. Luciferase activity was determined, and data are presented as RLU (mean ± SEM, n = 4).

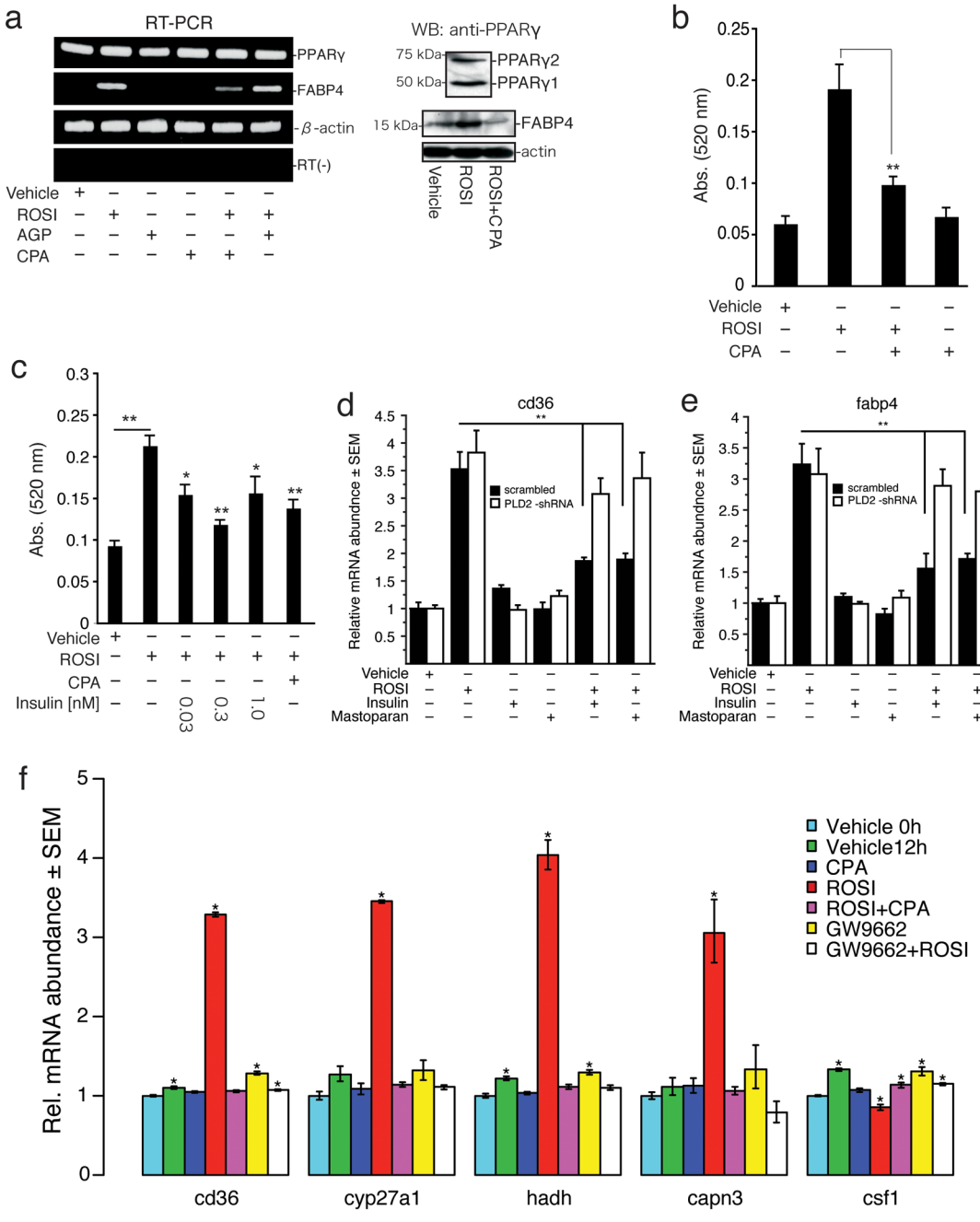

Figure 6. CPA inhibits PPARγ-dependent transcriptional responses

(a) 3T3-L1 cells, which express both PPARγ1 and PPARγ2 protein (western blotting inset), were pretreated with 1 μM CPA, AGP or vehicle for 24 h and exposed to 100 nM ROSI. Quantitative RT-PCR (QT-PCR) for the adipocyte marker *fabp4* was performed 5 days later.

(b) CPA inhibits ROSI-induced lipid accumulation. 3T3-L1 cells pretreated with 1 μM CPA or vehicle for 24 h were induced to differentiate with ROSI (100 nM every other day) and stained with ORO after 10 days. Quantification of lipid accumulation was done spectrophotometrically (n=3).

(c) Insulin or CPA inhibit lipid accumulation in 3T3-L1 cells. Cells were pretreated with 1 μM CPA or vehicle for 24 h and induced with 100 nM ROSI with or without 1 μM CPA or

insulin and stained with ORO after 2 weeks. Quantification of lipid accumulation was done spectrophotometrically (n=3, **p=0.0002 for DMSO *vs.* ROSI, *p=0.0126 for ROSI *vs.* ROSI+0.03 nM insulin, **p=0.0010 for ROSI *vs.* ROSI + 0.3 nM insulin, *p=0.0494 for ROSI *vs.* ROSI+1 nM Insulin, and **p=0.0041 for ROSI *vs.* ROSI+CPA).

(**d, e)** ROSI-induced gene expression of PPARγ target genes fabp4 and cd36 is inhibited by PLD2 in 3T3-L1 cells. 3T3-L1 cells expressing scrambled shRNA or PLD2 shRNA were pretreated with 30nM insulin or 10μM mastoparan for 30 min and cultured in ROSI (10 μM) or vehicle for 24 h. Total RNA was isolated and mRNA levels determined by QT-PCR (n=4).

(f) Inhibition of ROSI-induced expression of PPARγ regulated genes by CPA in mouse peritoneal macrophages. Macrophages isolated from C57BL/6 mice were exposed to a 5 μM ROSI with or without 5 μM CPA or 1 μM GW9662 (positive control) for 12 h, and RNA was isolated. mRNA levels for the PPARγ upregulated (*cd36*, *cyp27a1*, *hadh*, *capn3)* and downregulated *(csf1)* gene targets were determined by QT-PCR) (n=3, representative experiment shown).

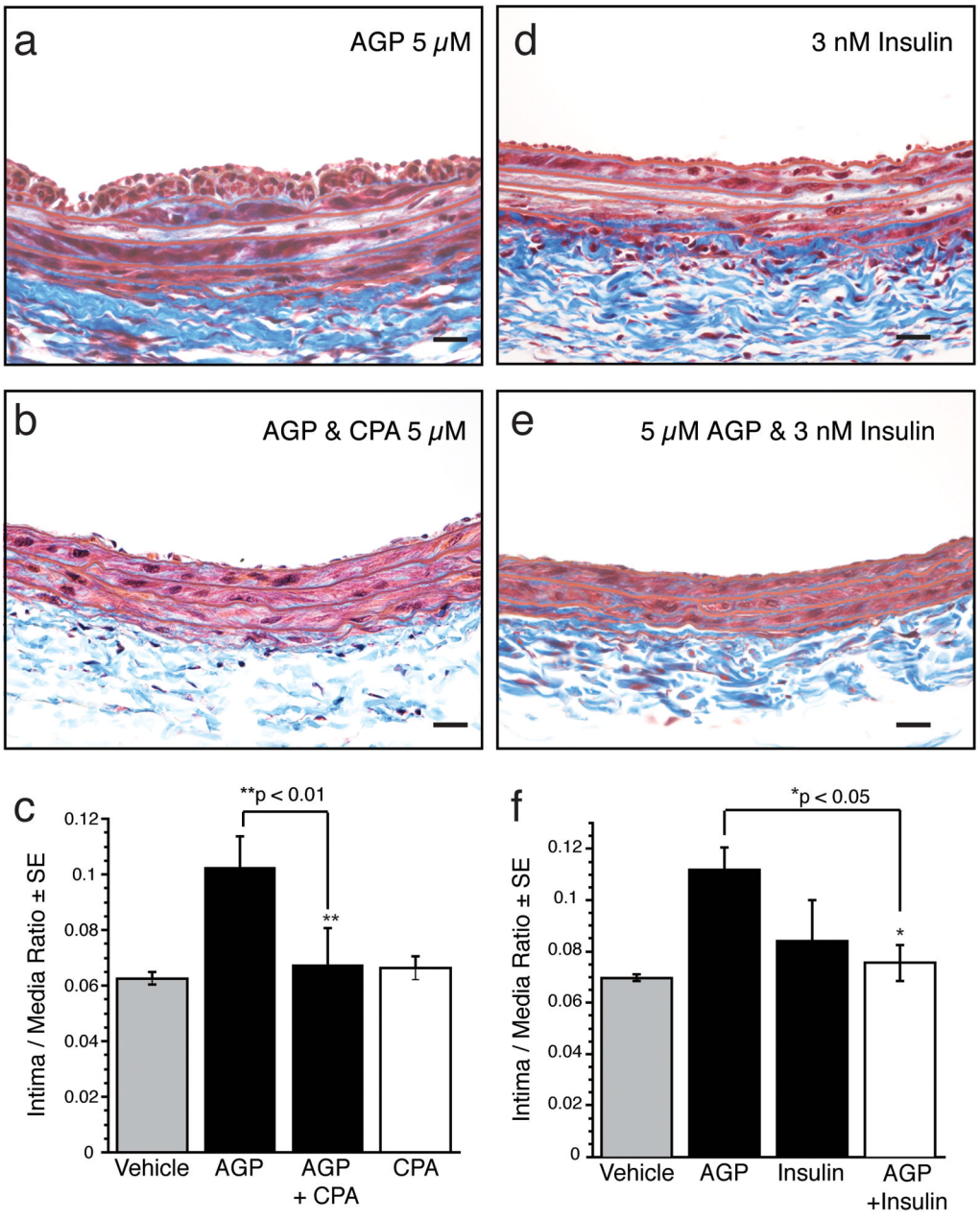

Figure 7. CPA and insulin prevent carotid wall remodeling

(a–b) Carotid arteries of anesthetized adult rats (5 per group) were exposed to 5 μM AGP alone (a) or with 5 μM CPA (b) for 1 h. (Masson trichrome staining, bar 200 μm).

(c) CPA treatment blocks increase in intima-to-media ratios AGP-induced rat carotid arteries (n=5 per group).

(d–f) Insulin (3 nM) was applied alone (d) or with 5 μM AGP (e) intralumenally for 1 h and neointima formation assessed three weeks alters. bar 200 μm. (f) Quantification of intima/media ratios (n=5).